Sedimentation profiles of polydisperse fluids

2003 J. Phys.: Condens. Matter 15 5417

(http://iopscience.iop.org/0953-8984/15/32/303)

INSTITUTE OF PHYSICS PUBLISHING JOURNAL OF PHYSICS: CONDENSED MATTER

J. Phys.: Condens. Matter **15** (2003) 5417–5428 PII: S0953-8984(03)61563-8

Sedimentation profiles of polydisperse fluids

L Bellier-Castella and H Xu

Laboratoire de Physique de la Matière Condensée et Nanostructures (UMR 5586 du CNRS), Université Claude Bernard-Lyon1, 69622 Villeurbanne Cedex, France

E-mail: hxu@lpmcn.univ-lyon1.fr

Received 1 April 2003, in final form 6 June 2003
Published 1 August 2003
Online at stacks.iop.org/JPhysCM/15/5417

Abstract

The equilibrium sedimentation profiles of polydisperse van der Waals fluids have been calculated within the framework of the density functional theory of non-uniform polydisperse fluids. The main focus is on the delicate balance between the gravitational force, the interparticle attraction, and the excluded volume effects. In the presence of gravity, a polydisperse system will experience size segregation. This trend is reinforced when the polydispersity of the fluid is increased. The details of this size segregation are quite sensitive to how the different parts of the interparticle interactions depend on the polydispersity. In the present work, it is also shown that, within the local density approximation, the density profiles can be inverted to give the osmotic pressure. This suggests a practical way of measuring the equation of state of polydisperse colloidal dispersions.

1. Introduction

The study of sedimentation profiles of colloidal suspensions is an old subject which goes back to Perrin [1]. When using the approximation of non-interacting particles, the density profile will follow an exponential law, which allowed Perrin to measure Avogadro's number in a simple way. Deviations from the exponential law have motivated many authors. We can quote the systematic work of Vrij [2], who studied equilibrium density profiles of monodisperse and polydisperse hard sphere suspensions using the Percus–Yevick approximation. In the original work of Biben *et al* [3], the problem has been recast in the framework of the density functional theory of inhomogeneous fluids. In particular, it has been shown that, for smoothly varying density profiles, the use of the local density approximation (LDA) allows one to obtain the osmotic pressure via an inversion procedure. This result is very useful, since nowadays the density profile can be measured by optical methods [4–7]. The inversion procedure has thus been applied by Piazza *et al* [4] to obtain the equation of state of charge-stabilized colloidal particles. The DFT-LDA approach has also been applied to the sedimentation of binary hard sphere mixtures [3], and size segregation has been observed. Recently, the sedimentation

profiles of a rather complicated system—the star polymers—have been investigated [8]. However, the case of polydisperse fluids has scarcely been examined, probably because of the intrinsic complexity of polydisperse systems [9]. As polydispersity is always more or less present in colloidal preparations [10], it is thus interesting to observe its effect on the sedimentation profiles. This is the aim of the present work. It is an expansion of some preliminary results shown recently [11].

This paper is organized as follows: in section 2 we present the theoretical framework and the method to obtain the density profiles; section 3 is devoted to the osmotic pressure; the last section contains our conclusions.

2. Density functional theory for sedimentation profiles of polydisperse fluids

Consider a colloidal dispersion of spherical particles in a solvent. The system is contained in a tube with a semi-infinite geometry in the z-direction. The particles have radii $R(\sigma)$, where σ designates both the species label and the dimensionless polydispersity parameter, which is defined by $\sigma = R(\sigma)/R(1)$ (where $R(1)$ is a reference radius). We consider a continuous size distribution, i.e. $0 < \sigma < \infty$. Under the gravitational potential $\phi(z, \sigma) = m(\sigma)gz$, an inhomogeneous density profile $\rho(z, \sigma)$ builds up. The problem is most naturally cast in the framework of density functional theory [3], for which we briefly recall the formalism. With $\rho(\boldsymbol{r}, \sigma)$ coupled with the external potential $\phi(\boldsymbol{r}, \sigma)$, we can write down the Euler–Lagrange equation for the free-energy functional $F[\rho]$:

$$\mu(\sigma) = \phi(\boldsymbol{r}, \sigma) + \left.\frac{\delta F[\rho]}{\delta \rho(\boldsymbol{r}, \sigma)}\right|_{\mathrm{T}} \tag{1}$$

where $\mu(\sigma)$ is the chemical potential of the species σ. For van der Waals (vdW) polydisperse fluids [13], the intrinsic free-energy functional reads as

$$\begin{aligned} F(T, [\rho]) = k_{\mathrm{B}}T \int \mathrm{d}\boldsymbol{r} \int \mathrm{d}\sigma\, \rho(\boldsymbol{r}, \sigma) \left\{ \ln\left(\frac{\Lambda^3(\sigma)\rho(\boldsymbol{r}, \sigma)}{E(\boldsymbol{r}, [\rho])} \right) - 1 \right\} \\ + \tfrac{1}{2} \int \mathrm{d}\boldsymbol{r} \int \mathrm{d}\sigma \int \mathrm{d}\boldsymbol{r}' \int \mathrm{d}\sigma'\, \rho(\boldsymbol{r}, \sigma) V_{\mathrm{A}}(|\boldsymbol{r} - \boldsymbol{r}'|; \sigma, \sigma') \rho(\boldsymbol{r}', \sigma') \end{aligned} \tag{2}$$

where $\Lambda(\sigma)$ is the thermal de Broglie wavelength resulting from the kinetic energy and $E[\boldsymbol{r}, \rho]$ is the vdW excluded volume correction that results from the repulsions

$$E(\boldsymbol{r}, [\rho]) = 1 - \int \mathrm{d}\sigma\, v(\sigma)\rho(\boldsymbol{r}, \sigma). \tag{3}$$

The volume term $v(\sigma)$ generally depends on the polydispersity, as well as the interparticle attraction, $V_{\mathrm{A}}(|\boldsymbol{r} - \boldsymbol{r}'|; \sigma, \sigma')$. In the absence of experimental indication, we adopt—as explained in [12–14]—the simple model

$$v(\sigma) = v(1)\sigma^k \qquad V_{\mathrm{A}}(r; \sigma, \sigma') = \sigma\sigma' V_{\mathrm{A}}(r; 1, 1) \tag{4}$$

where $v(1) = (4\pi/3)R^3(1)$ and $k = 0$ or 1. The case $k = 0$ corresponds to the simple model where $v(\sigma)$ is independent of σ, as in [13], and $k = 1$ corresponds to where $v(\sigma)$ is linearly dependent on σ, as in [12]. The case $k = 3$ would be more realistic but numerically more difficult to tackle. In view of the z dependence only of ϕ and ρ, equation (1) becomes

$$\begin{aligned} \mu(\sigma) = \phi(z, \sigma) + k_{\mathrm{B}}T \ln \frac{\Lambda^3(\sigma)}{v(1)} + k_{\mathrm{B}}T \ln \frac{\eta(z, \sigma)}{1 - \eta_k(z)} + k_{\mathrm{B}}T \frac{\sigma^k \eta_0(z)}{1 - \eta_k(z)} + \sigma V_0 \eta_1(z) \\ + \sigma \int_{-\infty}^{\infty} \mathrm{d}z'\, V_1(|z - z'|)\{\eta_1(z') - \eta_1(z)\} \end{aligned} \tag{5}$$

where $\eta(z,\sigma) = v(1)\rho(z,\sigma)$ is a dimensionless local density,

$$v(1)V_1(|z|) = \int_{-\infty}^{\infty} \mathrm{d}x \int_{-\infty}^{\infty} \mathrm{d}y\, V_\mathrm{A}\Big(\sqrt{x^2+y^2+z^2}; 1, 1\Big) \tag{6}$$

is the z-dependent attraction term, and

$$v(1)V_0 = \int \mathrm{d}\boldsymbol{r}\, V_\mathrm{A}(r; 1, 1) = -8\epsilon(1,1)v(1) \tag{7}$$

is the cohesion energy of the reference system (where $\epsilon(1,1)$ is an energy scale).

We recall that

$$\eta_n(z) = \int \mathrm{d}\sigma\, \sigma^n \eta(z,\sigma) \qquad (n \geqslant 0) \tag{8}$$

are the nth moments of the dimensionless local density $\eta(z,\sigma)$.

In this work we assume that the spatial variation of $\eta(z,\sigma)$ is smooth over the range of $V_1(z)$ so that we can adopt the LDA, in which case the last term in equation (5) can be dropped. This leads to

$$\mu(\sigma) = \phi(z,\sigma) + k_\mathrm{B}T \ln \frac{\Lambda^3(\sigma)}{v(1)} + k_\mathrm{B}T \ln \frac{\eta(z,\sigma)}{1-\eta_k(z)} + k_\mathrm{B}T \frac{\sigma^k \eta_0(z)}{1-\eta_k(z)} + \sigma V_0 \eta_1(z). \tag{9}$$

Equation (9) can be rewritten in the form of an integral equation for $\eta(z,\sigma)$:

$$\eta(z,\sigma) = \left(\frac{v(1)}{\Lambda^3(\sigma)}\right)[1-\eta_k(z)] \exp\left[\beta\mu(\sigma) - \beta\phi(z,\sigma) - \frac{\sigma^k \eta_0(z)}{1-\eta_k(z)} - \beta V_0 \sigma \eta_1(z)\right] \tag{10}$$

where $\beta = 1/(k_\mathrm{B}T)$. When solving this equation, the following two constraints are to be satisfied:

(1) The boundary condition:

$$\lim_{z\to+\infty} \eta(z,\sigma) = 0. \tag{11}$$

(2) The particle number conservation of species σ:

$$\int_0^{\infty} \frac{\mathrm{d}z}{R(1)} \eta(z,\sigma) = \eta_\mathrm{s}(\sigma) \tag{12}$$

where $\eta_\mathrm{s}(\sigma)$ is a fixed (dimensionless) surface density distribution.

To solve equation (10), we can project it in moment space. This gives, for the first two orders,

$$\eta_0(z) = B_0(z) \int \mathrm{d}\sigma\, A_0(z,\sigma) \exp\left[-\beta\phi(z,\sigma) + \frac{8}{t}\sigma\eta_1(z) + \beta\mu(\sigma)\right] \tag{13}$$

$$\eta_1(z) = B_0(z) \int \mathrm{d}\sigma\, \sigma A_0(z,\sigma) \exp\left[-\beta\phi(z,\sigma) + \frac{8}{t}\sigma\eta_1(z) + \beta\mu(\sigma)\right] \tag{14}$$

where

$$B_0(z) = \{1-\eta_k(z)\}\frac{v(1)}{\Lambda^3(\sigma)} \qquad A_0(z,\sigma) = \exp\left[-\frac{\sigma^k\eta_0(z)}{1-\eta_k(z)}\right] \qquad (k = 0 \text{ or } 1) \tag{15}$$

and $t = k_\mathrm{B}T/\epsilon(1,1) = -8k_\mathrm{B}T/V_0$ is the reduced temperature. The system of equations (13) and (14) can be solved jointly with the constrains (11) and (12). The model of an excluded volume independent of the polydispersity, $v(\sigma) = v(1)$ (i.e. $k = 0$), offers a great simplification of the solution method because, in this case, A_0 in equations (13) and (14) becomes independent of σ. We can thus divide (13) by (14), which gives

$$\eta_0(z) = \eta_1(z)\frac{\int \mathrm{d}\sigma\, C[z,\sigma,\eta_1(z)]}{\int \mathrm{d}\sigma\, \sigma C[z,\sigma,\eta_1(z)]} \tag{16}$$

where

$$C[z,\sigma,\eta_1(z)] \equiv \exp\left[-\beta\phi(z,\sigma)+\frac{8}{t}\sigma\eta_1(z)+\beta\mu(\sigma)\right]. \tag{17}$$

Substituting equation (16) into (14), we obtain a closed integral equation for $\eta_1(z)$:

$$\eta_1(z) = B_0(z;\eta_0[\eta_1])A_0(z;\eta_0[\eta_1])\int \mathrm{d}\sigma\,\sigma\exp\left[-\beta\phi(z,\sigma)+\frac{8}{t}\sigma\eta_1(z)+\beta\mu(\sigma)\right]. \tag{18}$$

The chemical potential $\mu(\sigma)$ is fixed by constraint (12). In order to keep the problem tractable, we assume the following n-parameter ($1 < n < 6$) form for $\mu(\sigma)$:

$$\beta\mu(\sigma) = \ln\left(\frac{\Lambda^3(\sigma)}{v(1)}\right)+\ln(\eta_s(\sigma))+\sum_{i=0}^{n} a_i(\sigma-1)^i. \tag{19}$$

The n coefficients $\{a_i\}$ are then found by minimizing the norm function:

$$|\Delta\eta(\sigma)| = \left|\int_0^\infty \frac{\mathrm{d}z}{R(1)}\eta(z,\sigma)-\eta_s(\sigma)\right|. \tag{20}$$

In practice, $n = 4$ is sufficient to achieve a norm convergence to the order of 10^{-5} (meaning that the maximum value of $|\Delta\eta(\sigma)|$ is of the order of 10^{-5}). The effective mass of the colloidal particle, $m(\sigma)$, can be either dependent on or independent of the particle radius $R(\sigma)$, according to the particle's chemical composition [3]. In the present work, we studied two situations: $m(\sigma) = m(1)\sigma^l$, with $l = 0$ or 1 ($m(1)$ is a reference mass). The more realistic case with $l = 3$ is not considered, to avoid convergence difficulties in solving (18). As for the initial polydispersity distribution, i.e. $h_i(\sigma) = \eta_s(\sigma)/\eta_s$ ($\eta_s = \int \mathrm{d}\sigma\,\eta_s(\sigma)$), the Schulz distribution is adopted [13]:

$$h_i(\sigma) = \frac{\alpha^\alpha}{\Gamma(\alpha)}\sigma^{\alpha-1}\exp(-\alpha\sigma) \tag{21}$$

where $\Gamma(\alpha)$ is the Euler gamma function, $1/\alpha$ is the distribution's variance, and $I = 1+(1/\alpha)$ is the polydispersity index. From (21), we have the first two moments, $m_0^{(i)} = m_1^{(i)} = 1$ ($m_n^{(i)} = \int \sigma^n h_i(\sigma)\,\mathrm{d}\sigma$).

To summarize, the external parameters are the (reduced) temperature t, the initial density distribution $\eta_s(\sigma)$, the gravitational strength $\gamma = m(1)gR(1)/k_BT$, and the model parameters, which are k (for $v(\sigma)$) and l (for $m(\sigma)$). Once these are given, the iterative procedure (for $k = 0$) is the following: (1) A test set $\{a_i\}$ is proposed, giving $\mu(\sigma)$ through equation (19); (2) equation (18) is solved iteratively by the method of Ng [15], giving a first solution for $\eta_1(z)$. From $\eta_1(z)$, one obtains $\eta_0(z)$ from equation (16) and the profile $\eta(z,\sigma)$ from equation (10). (3) The norm function (20) is then evaluated. If its maximum value is smaller than a tolerance (here 5×10^{-5}), then $\eta(z,\sigma)$ is the searched profile. Otherwise, a new set of $\{a_i\}$ is given in view of minimizing (20)[1] and we return to point (1). For $k \neq 0$, point (2) will be different (see below). Because of this somewhat lengthy procedure, we only studied two values of the gravity parameter γ, i.e. $\gamma = 0.05$ and 0.1. Within this range, the only role of γ seems to be controlling the decay of $\eta(z,\sigma)$ at large z, which follows the ideal gas law $\eta(z,\sigma) \propto \exp[-\gamma\sigma^l z/R(1)]$ for $z \gg R(1)$. Although these γ values are rather weak compared to other theoretical studies of sedimentation profiles [3, 8], they are nevertheless quite significant for typical colloids [4]. In the following paragraph we shall examine some representative results that we obtained.

Figure 1 shows the density profile $\eta(z,\sigma)$ for a gravity parameter $\gamma = 0.1$, temperature $t = 1.5$, $m(\sigma) = m(1)$ and $v(\sigma) = v(1)$, compared with the monodisperse density profile $\eta_{\mathrm{mono}}(z)$. One clearly observes a segregation phenomenon. Instead of being a continuously

[1] NAG library, subroutine E04FCF.

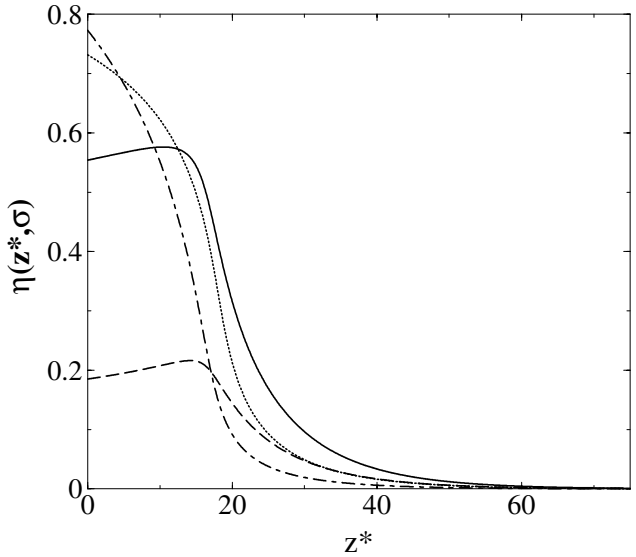

Figure 1. Reduced density profiles $\eta(z^\star, \sigma)$ as a function of the reduced distance $z^\star = z/R(1)$ of a polydisperse fluid with reduced surface density $\eta_s = \rho_s v(1)/R(1) = 13$, polydispersity index $I = 1.04$ at reduced temperature $t = k_B T/\epsilon(1, 1) = 1.5$, and the gravitational strength $\gamma = m(1)gR(1)/k_B T = 0.1$. The model that was used is $v(\sigma) = v(1)$ and $m(\sigma) = m(1)$. The curves represent three sizes: $\sigma = 1.25$ (— · —); 0.75 (——); and 0.65 (– – –). For comparison, the profile for a monodisperse system is also shown (· · ·).

decreasing function of z, the smaller particles ($\sigma < 1$) show a depletion at the bottom and some maximum density at a finite height. This can be understood by considering the combination of gravity (equal for all sizes) and the strong attraction among the larger spheres ($\sigma > 1$) that 'glue' the large spheres near the bottom and thus expel the smaller spheres from it. To support this analysis, we plot in figure 2 the density profiles at the current temperature ($t = 1.5$) and at very high temperature, where attractions no longer play any role. We see that, without attractions, the density profiles are much more spread out for all sizes and those for the smaller spheres are now continuously decreasing functions of z. It is also interesting to observe how the polydispersity influences the size segregation. In figure 3, we plot $\eta(z, \sigma)$ of the small spheres for two different values of I. Whereas for $I = 1.02$ the depletion phenomenon is just barely visible, for $I = 1.04$ it becomes quite important. Furthermore, if we allow $m(\sigma)$ to depend on σ, i.e. $m(\sigma) = m(1)\sigma$, then the size segregation is more pronounced (figure 4) because the gravitation and attraction act together to favour the situation with many large particles at the bottom. In figure 4, we compare the density profiles obtained from the two models of $m(\sigma) = m(1)\sigma^l$, i.e. $l = 0$ and 1. Those with $l = 1$ indeed give an increased density of the large spheres at the bottom and enhance the depletion of the small spheres. This kind of size segregation has also been observed in binary hard sphere mixtures [3], but only in the case of a strong dependence of the effective mass on the particle size, i.e. $m(\sigma) = m(1)\sigma^3$, and not in the case $m(\sigma) = m(1)$, as in our study. This difference with respect to our results is easily understood if we remember that, in binary hard sphere mixtures, there is no attraction term and the excluded volume is proportional to R_i^3 ($i = 1, 2$). Thus, the size segregation is controlled by the balance between gravity and the excluded volume terms only. If we render our model more realistic by installing a dependence of the excluded volume on σ, then the balance between the volume exclusion and the attraction appears in our system. We would lose

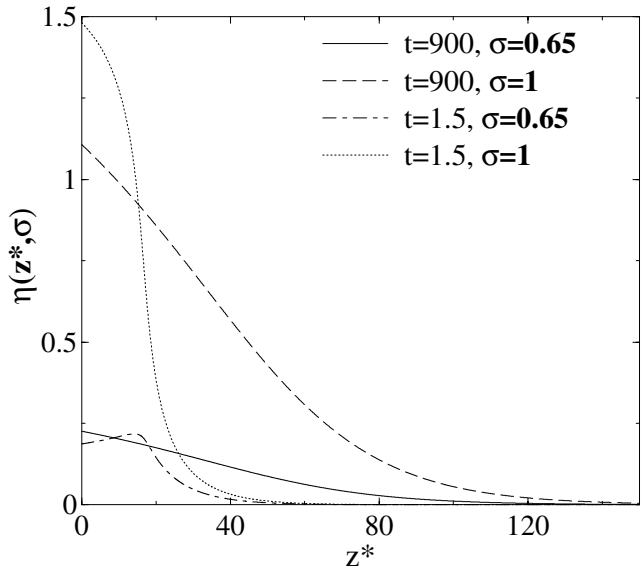

Figure 2. A comparison of the density profiles $\eta(z^\star, \sigma)$ at $t = 1.5$ and at very high temperature $t = 900$ (limit $t \to \infty$) for $\sigma = 0.65$ and 1. These profiles correspond to $\gamma = 0.05$, $I = 1.04$ and $\eta_s = 25$. The model used is $v(\sigma) = v(1)$ and $m(\sigma) = m(1)$.

the numerical simplicity of the $k = 0$ model, since equations (13) and (14) must now be solved simultaneously, making convergence to the solution much more difficult. Nevertheless, it can be reached in some cases. As an example, in figure 5 we show density profiles with or without a polydispersity-dependent excluded volume, i.e. $v(\sigma) = v(1)$ or $v(1)\sigma$, with $m(\sigma) = m(1)$. The effect of volume polydispersity is very visible: for $k = 0$ the density of large spheres is a continuously decreasing function of z whereas that of the small spheres is not (see the inset). We are in an 'attraction dominant' situation. In contrast, for $k = 1$ the tendencies are inverted, i.e. the small spheres adopt a continuously decreasing density profile and the large spheres adopt a non-continuous profile now, as in the binary hard sphere mixture [3] when $m(\sigma) = m(1)$. The weak polydispersity index used here ($I = 1.02$) did not allow us to observe a clear depletion of the large spheres, but the trend is there (see the inset). By using optical measurements [4–7] it is possible to determine density profiles at a given z and analyse the size distribution. This would then indicate how the interaction potential depends on the polydispersity. In figure 6, we show typical results for the moment profiles $\eta_0(z)$ and $\eta_1(z)$, within the model $m(\sigma) = m(1)\sigma$. We see that they are continuous functions of z. But there is an indication of size segregation. The initial distribution has $m_1^{(i)} = 1$. If we define a local first moment $m_1(z) = \eta_1(z)/\eta_0(z)$, then near the bottom we have $m_1(z) > 1$ and above a certain height ($z \approx 20R(1)$) we have $m_1(z) < 1$ (see inset). However, unlike the local densities, the moments only display quite slight segregation here due to the integration over σ. Before closing this section we note that, in a theoretical study of polydisperse hard sphere fluids near a wall [16], a local size segregation has also been predicted.

3. Equation of state from the density profiles

Here we show a general approach for obtaining the osmotic pressure from the (measured or theoretical) sedimentation density profiles. It is a generalization to the polydisperse case of

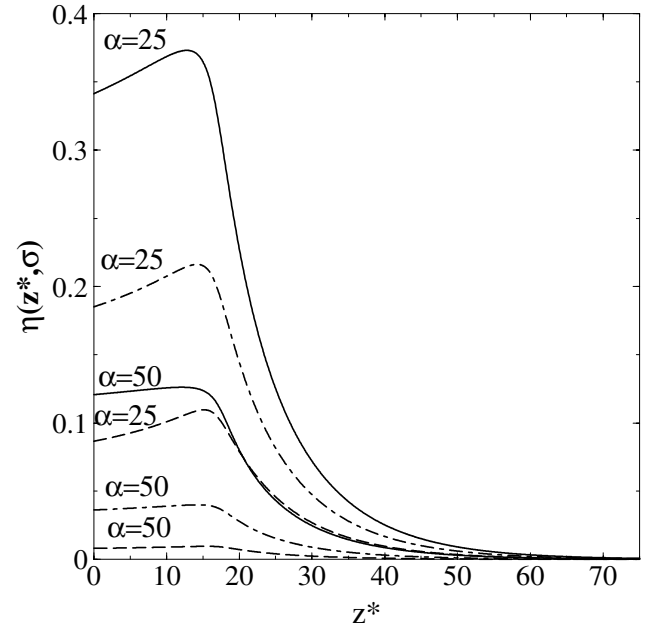

Figure 3. The influence of the polydispersity index I on the density profiles of the small particles. Displayed here are the profiles $\eta(z^\star, \sigma)$ corresponding to $I = 1.04$ (or $\alpha = 25$) and $I = 1.02$ (or $\alpha = 50$) for particle sizes $\sigma = 0.7$ (——), 0.65 (— · —) and 0.6 (– – –). The thermodynamic conditions t, η_s and γ are identical to those of figure 1.

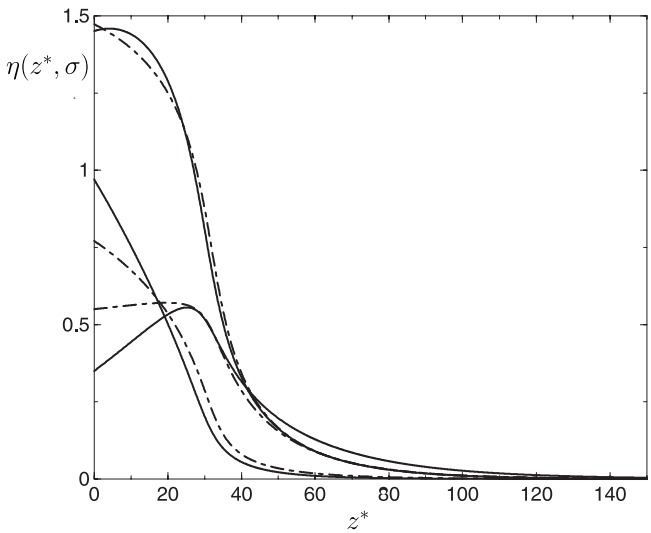

Figure 4. The influence of the *mass* polydispersity on the density profiles $\eta(z^\star, \sigma)$. The first case corresponds to $m = m(1)$ (— · —) and the second to $m = m(1)\sigma$ (——). For each case, three sizes are shown: $\sigma = 1$ (top curve), 1.25 (middle curve) and 0.75 (lower curve). The polydispersity index $I = 1.04$ and the thermodynamic conditions are $\eta_s = 25$, $t = 1.5$ and $\gamma = 0.05$. Here, $v(\sigma) = v(1)$.

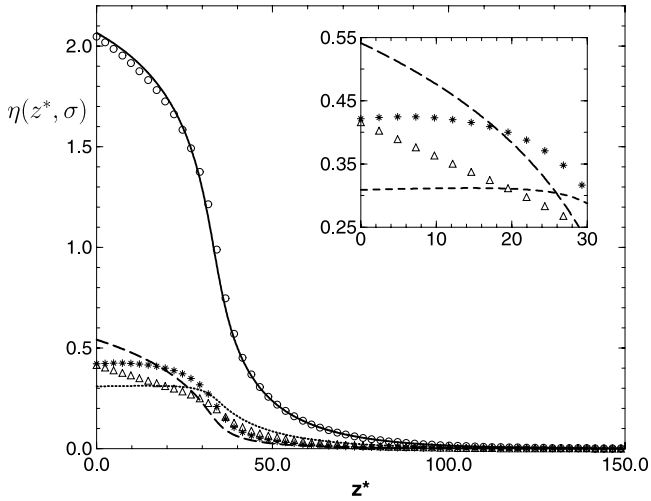

Figure 5. The influence of *volume* polydispersity on the density profiles $\eta(z^\star, \sigma)$. The polydispersity index $I = 1.02$ and the thermodynamic conditions are $\eta_s = 25$, $t = 1.5$ and $\gamma = 0.05$. The mass polydispersity is $m(\sigma) = m(1)$. The first model is $v = v(1)$; profiles shown correspond to $\sigma = 1$ (——), 1.25 (– – –) and 0.75 (· · · · · ·). The second model is $v = v(1)\sigma$; profiles shown correspond to $\sigma = 1$ (circles), 1.25 (stars) and 0.75 (triangles). The inset shows a blow-up of the large ($\sigma = 1.25$) and small ($\sigma = 0.75$) particle distributions near the bottom ($0 \leqslant z^* \leqslant 30$).

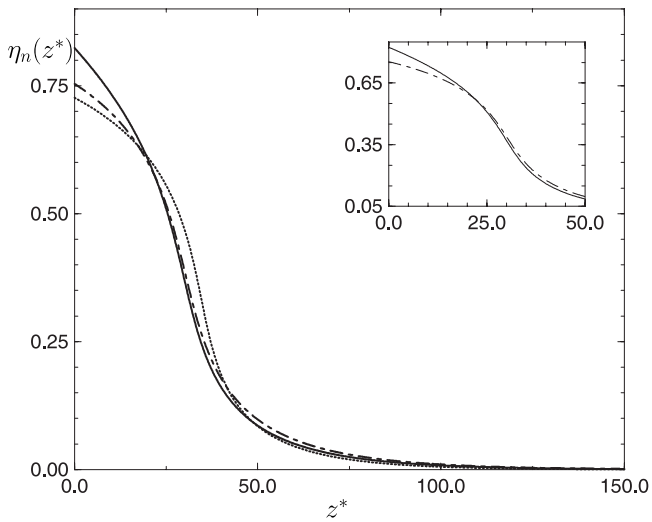

Figure 6. Moment profiles $\eta_0(z^*)$ (— · —) and $\eta_1(z^*)$ (——) for $I = 1.04$ (i.e. $\alpha = 25$). The model corresponds to $m(\sigma) = m(1)\sigma$ and $v(\sigma) = v(1)$. The thermodynamic conditions are $\eta_s = 25$, $t = 1.5$ and $\gamma = 0.05$. The monodisperse density profile $\eta_{\text{mono}}(z^*)$ (· · · · · ·) is also shown. The inset shows $\eta_0(z^*)$ and $\eta_1(z^*)$ for $0 \leqslant z^* \leqslant 50$.

the inversion procedure, presented in [3]. We start from the intrinsic free-energy functional within the LDA:

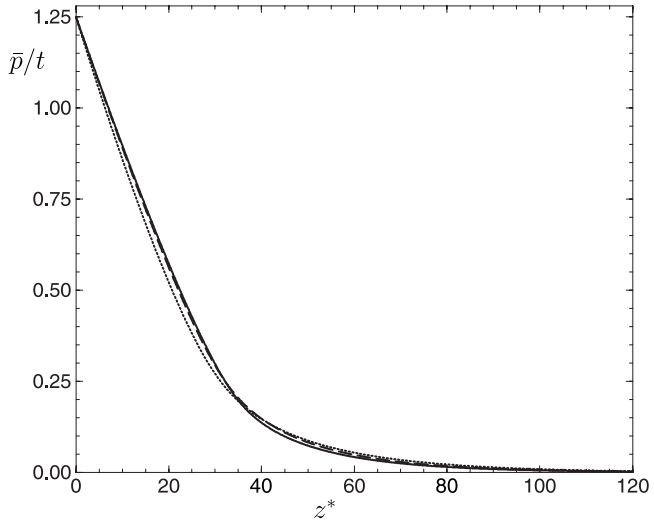

Figure 7. The influence of the polydispersity on the pressure profile $\bar{p}(z^*)$. We compare the monodisperse curve (——) with those of polydisperse fluids having $I = 1.04$ and corresponding to two models: $m = m(1)$ (– – –) and $m = m(1)\sigma$ (· · · · · ·). Here we have $\eta_s = 25$, $t = 1.5$, $\gamma = 0.05$ and $v(\sigma) = v(1)$.

$$F(T, [\rho]) = \int \mathrm{d}\boldsymbol{r}\, f = \int \mathrm{d}\boldsymbol{r} \int \mathrm{d}\sigma\, f_{\mathrm{i}}(T, \rho(\boldsymbol{r}, \sigma)) + \int \mathrm{d}\boldsymbol{r}\, f_{\mathrm{ex}} \tag{22}$$

where the first term (f_{i}) corresponds to the ideal part and the second term (f_{ex}) corresponds to the excess part of the free energy. The expression of f_{i} is

$$f_{\mathrm{i}}(T, \rho(\boldsymbol{r}, \sigma)) = k_{\mathrm{B}}T\rho(\boldsymbol{r}, \sigma)\{\ln(\Lambda^3(\sigma)\rho(\boldsymbol{r}, \sigma)) - 1\} \tag{23}$$

and, within our vdW model, the expression of f_{ex} is given by

$$f_{\mathrm{ex}}(T, \eta_0(\boldsymbol{r}), \eta_1(\boldsymbol{r})) = -\frac{k_{\mathrm{B}}T}{v(1)}\eta_0(\boldsymbol{r})\ln(1 - \eta_k(\boldsymbol{r})) + \frac{1}{2v(1)}\eta_1^2(\boldsymbol{r})V_0 \qquad (k = 0 \text{ or } 1). \tag{24}$$

We notice that f_{i} is local in $\rho(\boldsymbol{r}, \sigma)$ (depending on $\boldsymbol{r}$ and σ through $\rho(\boldsymbol{r}, \sigma)$), whereas f_{ex} (within the LDA) is a local function of the first few *moments* of $\rho(\boldsymbol{r}, \sigma)$. If we assume that thermodynamics can be applied locally (this is consistent with LDA), then the osmotic pressure is related to F in the following way:

$$\Pi(\boldsymbol{r}) = \int \mathrm{d}\sigma\, \rho(\boldsymbol{r}, \sigma)\frac{\delta F}{\delta\rho(\boldsymbol{r}, \sigma)} - f = \int \mathrm{d}\sigma\, \rho(\boldsymbol{r}, \sigma)\frac{\delta F}{\delta\rho(\boldsymbol{r}, \sigma)} - \left[\int \mathrm{d}\sigma\, f_{\mathrm{i}}(T, \rho(\boldsymbol{r}, \sigma)) + f_{\mathrm{ex}}(T, \eta_0(\boldsymbol{r}), \eta_1(\boldsymbol{r}))\right]. \tag{25}$$

As Π is only z-dependent, we rewrite (25) as

$$\Pi(z) = \int \mathrm{d}\sigma\, \rho(z, \sigma)\frac{\delta F}{\delta\rho(z, \sigma)} - \left[\int \mathrm{d}\sigma\, f_{\mathrm{i}}(T; \rho(z, \sigma)) + f_{\mathrm{ex}}(T, \eta_0(z), \eta_1(z))\right]. \tag{26}$$

After substituting the Euler–Lagrange equation (1) into the first part of equation (26), and then taking the z derivative of the latter, Π can be related to the sedimentation profiles $\rho(z, \sigma)$ in the simple way

$$\frac{\mathrm{d}\Pi}{\mathrm{d}z} = -\int \mathrm{d}\sigma\, \rho(z, \sigma)m(\sigma)g. \tag{27}$$

We notice that equation (27) is the well known macroscopic osmotic equilibrium condition [17], applied here to polydisperse fluids. The above demonstration, from equations (22) to (27), is valid as long as the free-energy functional F can be expressed as the integral of a local function of z through the local density $\rho(z, \sigma)$. The pressure on the bottom wall (at $z = 0$) is deduced by integration of (27) between $z = 0$ and ∞ and using the boundary condition $\Pi(+\infty) = 0$, which gives

$$\Pi(0) = \int \mathrm{d}\sigma\, m(\sigma) g \int_0^\infty \mathrm{d}z\, \rho(z, \sigma) = \int \mathrm{d}\sigma\, m(\sigma) g \rho_\mathrm{s}(\sigma) \tag{28}$$

where $\rho_\mathrm{s}(\sigma)$ is the density per cross-sectional area for the σ species. The pressure profile is thus given by:

$$\Pi(z) = \int \mathrm{d}\sigma\, m(\sigma) g \rho_\mathrm{s}(\sigma) - \int \mathrm{d}\sigma\, m(\sigma) g \int_0^z \mathrm{d}z'\, \rho(z', \sigma). \tag{29}$$

For example, if we take $m(\sigma) = m(1)\sigma^l$ ($l = 0, 1$), then

$$\bar{p}(z) = \gamma t \int \mathrm{d}\sigma\, \sigma^l \eta_\mathrm{s}(\sigma) - \gamma t \int_0^z \frac{\mathrm{d}z'}{R(1)} \int \mathrm{d}\sigma\, \sigma^l \eta(z', \sigma) \tag{30}$$

where $\bar{p} = \Pi v(1)/\epsilon(1, 1)$. For $m(\sigma) = m(1)$, the pressure is obtained by integrating $\eta_0(z)$:

$$\bar{p}(z) = \gamma t \eta_\mathrm{s} - \gamma t \int_0^z \frac{\mathrm{d}z'}{R(1)} \eta_0(z') \tag{31}$$

whereas, for $m(\sigma) = m(1)\sigma$, we have

$$\bar{p}(z) = \gamma t \int \mathrm{d}\sigma\, \sigma \eta_\mathrm{s}(\sigma) - \gamma t \int_0^z \frac{\mathrm{d}z'}{R(1)} \eta_1(z'). \tag{32}$$

In figure 7, we show $\bar{p}(z)$ versus z for $I = 1.04$ and the two models of $m(\sigma)$. As a function of z, the pressure profiles turn out to be quite close to the monodisperse case. This is a consequence of $\eta_0(z)$ and $\eta_1(z)$ being close to the monodisperse $\eta(z)$ (see figure 6). To check the inversion procedure, we have compared the values of $\bar{p}\,(t; \eta_0(z), \eta_1(z))$ from (31) and (32) to the local vdW equation of state:

$$\bar{p}_\mathrm{vdW}(t; \eta_0(z), \eta_1(z)) = \frac{t\eta_0(z)}{1 - \eta_k(z)} - 4\eta_1^2(z) \qquad (k = 0 \text{ or } 1) \tag{33}$$

and noticed that they indeed fall on the surface defined by (33). This is true for $k = 0$ and 1. Of course, the equation of state of a homogeneous polydisperse vdW fluid depends strongly on the k-value in the excluded volume $v(\sigma) = v(1)\sigma^k$. To show this, in figure 8 we plot the pressure versus the average density η_0 of a homogeneous vdW fluid with slightly different η_1 and for the two models of the excluded volume. We indeed observe quite different curves. Therefore, the inversion procedure defined by equation (29) allows one to deduce $\Pi(T; \eta_0, \eta_1)$ from measured density profiles and compare it with theoretical equations (Percus–Yevick, vdW, etc) to find out how the different parts of the interactions depend on the polydispersity.

4. Conclusions

In this work we studied the sedimentation profiles of polydisperse vdW fluids within the DFT-LDA formalism. By accurately solving the integral equations for the moments of the local density $\rho(z, \sigma)$, we were able to observe interesting size segregation phenomena, monitored by the interplay between gravitation, interparticle attractions and repulsions. It is also shown that, within the LDA, an inversion procedure exists, which allows the osmotic equation of state to be obtained from the knowledge of the density profile $\rho(z, \sigma)$. These results could

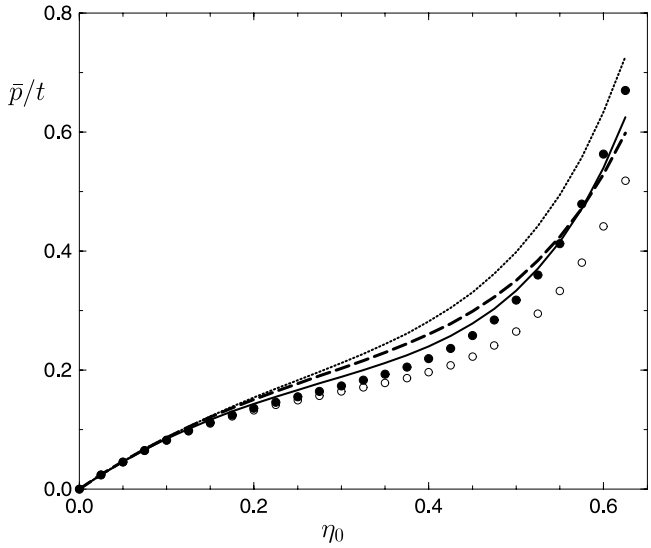

Figure 8. The equation of state $\bar{p}(t;\eta_0,\eta_1)$, given by equation (33), of a homogeneous vdW fluid, for $t = 1.5$. Two models considered are (i) $v(\sigma) = v(1)$ and (ii) $v(\sigma) = v(1)\sigma$. For the first model we show fluids with $m_1 = 0.95$ ($\cdots\cdots$) and 1.05 (circles); for the second model we show fluids with $m_1 = 0.95$ ($---$) and 1.05 (dots). We recall that $m_1 = \eta_1/\eta_0$ is the first moment of the size distribution $h(\sigma)$. The monodisperse case is also shown (——).

of course be used in experiments, to determine the nature of the interparticle interactions and their dependence on the polydispersity of the sample. For technical reasons, the present study is limited to relatively weak gravitational strengths ($\gamma \leqslant 0.1$), low fluid density, and weak dependence of the particle volume and mass on the polydispersity. These technical points can be improved, yielding stronger effects than those observed here, but we believe we have captured the main qualitative features. One last point is that we deliberately avoided fluid–fluid phase separation by placing the system above its critical point, in order to keep the investigation within the framework of the LDA. The latter would naturally break down if a liquid–vapour interface existed in the system. It is of course possible to go beyond the LDA [3, 14], but the calculations would be much more involved and outside the scope of this study.

Acknowledgment

The authors would like to thank M Baus for helpful discussions.

References

[1] Perrin J 1910 *J. Physique* **9** 5
Perrin J 1914 *C. R. Acad. Sci., Paris* **158** 1168
[2] Vrij A 1980 *J. Chem. Phys.* **72** 3735
[3] Biben T, Hansen J P and Barrat J L 1993 *J. Chem. Phys.* **98** 7330
[4] Piazza R, Bellini T and Degiorgio V 1993 *Phys. Rev. Lett.* **48** 71
[5] Hunt N, Jardine R and Bartlett P 2000 *Phys. Rev.* E **62** 900
[6] de Hoog E H A, Kegel W K, van Blaaderen A and Lekkerkerker H N W 2001 *Phys. Rev.* E **64** 021407
[7] Weeks E R and Weitz D A 2002 *Phys. Rev. Lett.* **89** 095704
[8] Dzubiella J, Harreis H M, Likos C N and Löwen H 2001 *Phys. Rev.* E **64** 011405
[9] Sollich P 2002 *J. Phys.: Condens. Matter* **14** R79

[10] Poon W C K and Pusey P N 1995 *Observation, Prediction and Simulation of Phase Transitions in Complex Fluids* ed M Baus, L F Rull and J P Ryckaert (Dordrecht: Kluwer–Academic)
Pusey P N 1991 *Liquids, Freezing and Glass Transition* ed J P Hansen, D Levesque and J Zinn-Justin (Amsterdam: North-Holland) p 763
[11] Xu H, Bellier-Castella L and Baus M 2002 *J. Phys.: Condens. Matter* **14** 12147
[12] Gualtieri J A, Kincaid J M and Morrison G 1982 *J. Chem. Phys.* **77** 521
[13] Bellier-Castella L, Xu H and Baus M 2000 *J. Chem. Phys.* **113** 8337
[14] Bellier-Castella L, Xu H and Baus M 2002 *Phys. Rev.* E **65** 021503
[15] Ng Kin-Chue 1974 *J. Chem. Phys.* **61** 2680
[16] Pagonabarraga I, Cates M E and Ackland G J 2000 *Phys. Rev. Lett.* **84** 911
[17] Yang A J M, Fleming P D and Gibbs J H 1977 *J. Chem. Phys.* **67** 74